Physics of Fluids

RESEARCH ARTICLE | MARCH 13 2024

Vortex synchronization-enabled heat-transfer enhancement in a channel with backward- and forward-facing steps

Yuan Ma ; Feng Ren ; Hui Tang ; Chenglei Wang

Physics of Fluids 36, 033616 (2024)
https://doi.org/10.1063/5.0197059

Physics of Fluids ARTICLE pubs.aip.org/aip/pof

Vortex synchronization-enabled heat-transfer enhancement in a channel with backward- and forward-facing steps

Cite as: Phys. Fluids **36**, 033616 (2024); doi: 10.1063/5.0197059
Submitted: 11 January 2024 · Accepted: 25 February 2024 ·
Published Online: 13 March 2024

Yuan Ma,[1,a] Feng Ren,[2,a] Hui Tang,[1,a] and Chenglei Wang[1,3,b]

AFFILIATIONS

[1]Department of Mechanical Engineering, The Hong Kong Polytechnic University, Hong Kong, China
[2]School of Marine Science and Technology, Northwestern Polytechnical University, Xi'an, Shaanxi 710072, China
[3]The Hong Kong Polytechnic University Shenzhen Research Institute, Shenzhen, Guangdong 518057, China

[a]Electronic addresses: yuan1ma@polyu.edu.hk, renfeng@nwpu.edu.cn, and h.tang@polyu.edu.hk
[b]Author to whom correspondence should be addressed: chenglei.wang@polyu.edu.hk

ABSTRACT

A channel with one backward-facing step and one forward-facing step is a typical configuration in engineering applications. In the channel, good heat transfer performance is often required, and the enhancement is usually achieved by employing different passive control methods, such as modification of geometric configuration or application of nanofluid. However, the other control method, i.e., active flow control (AFC), which is likely more effective, has been rarely applied in such a scenario. This study aims to bridge this gap by exploring how a rigid plate affects the heat transfer of the channel. The plate either is stationary or actively rotates, corresponding to passive flow control or AFC. The influences of the horizontal position of the plate (S) and its orientation angle (θ) on the heat transfer performance are studied when the plate is stationary to provide a baseline. Compared to the baseline, the effects of S, θ, and the rotation frequency (f_r) are revealed when the plate undergoes a sinusoidal rotation. Such a thermo-fluid dynamic problem is numerically simulated by the immersed-boundary lattice Boltzmann method. The results show that the plate can improve the heat transfer performance no matter whether it rotates or not, compared to the case without a plate. The rotating plate outperforms the stationary one when θ and f_r are properly chosen at each S. Substantial improvement can be achieved when vortex synchronization or resonance occurs in the channel, i.e., when the natural vortex shedding frequency is close or equal to f_r.

I. INTRODUCTION

A channel with either backward-facing steps (BFSs) or forward-facing steps (FFSs), or both, has been extensively applied in various engineering applications,[1,2] such as combustion chambers,[3] electronics cooling systems,[4] energy systems,[5] heat exchangers,[6] etc. In such a channel, a high heat transfer rate is usually required, for which different strategies have been adopted.

One popular approach is to modify the geometric configuration of the channel, including changing its shape or orientation and placing some additional solid structures in it, such as a plate, a baffle, or a blockage structure.[7,8] For example, Mohammed *et al.*[9] numerically studied the effects of blockage structures of various shapes on the flow and heat transfer in a channel with a BFS at $50 \leq Re \leq 200$, where Re is the Reynolds number. A circular, a back-facing triangular, a front-facing triangular, and a trapezoidal blockage body were considered, respectively. They found that the front-facing triangle can result in the best heat transfer performance with a 32% enhancement. Li *et al.*[10] fixed a porous plate on the top wall of a channel with a BFS, aiming at improving its heat transfer performance at $100 \leq Re \leq 500$. They found that the performance can be enhanced when the plate length increases or when the porous medium is less permeable. Jalil *et al.*[11] used a turbulator for improving the heat transfer performance of the channel with an FFS in the range of $5000 \leq Re \leq 10\,000$. Different turbulator shapes have been considered, including elliptical, trapezoidal, triangular, and curvy turbulators. They found that the turbulator shape significantly influences the heat transfer performance, and the best one can be achieved when the trapezoidal turbulator is applied. Xie and Xi[12] explored the forced convection over backward- and forward-facing steps (BFFS) at $Re = 700$. They found that the bottom-wall length has a notable influence on the flow dynamics and the heat

transfer performance in the reattachment region, which increases by about 10% when the length is 12 times the inlet height. Issakhov *et al.*[13] mainly investigated the effects of the inclination angle of a channel with BFFS on the mixed-convection heat transfer when $Re = 100$, $Pr = 0.7$, and $Gr = 609$, where Pr is the Prandtl number and Gr is the Grashof number. It was found that the inclination angle determines how the buoyancy force affects the shape of the recirculation region, and the temperature approaches the maximum in the middle of the channel at the inclination angle of 150°, 180°, and 210°. Atashafrooz and Nassab[14] studied how the inclination angle of the steps affect the heat transfer of a channel with BFFS at $Re = 400$ and $Pr = 0.71$, when combined convection and radiation are involved. The outcomes demonstrate that the maximum Nusselt number increases by increasing the inclination angle from 10° to 90°. Rehman *et al.*[15] numerically studied the effects of two partially heated circular obstacles on the heat transfer performance in a channel with double FFS at $Re = 20$ and $Pr = 1.5$. They observed that when the two obstacles are placed distantly, a higher Nusselt number along the first step can be obtained. Hilo *et al.*[16] numerically investigated the effects of corrugated shapes of the bottom wall in a channel with FFS at $5000 \leq Re \leq 20\,000$, including smooth, triangular, trapezoidal, and zigzag corrugated shapes. The results show that trapezoidal corrugated wall can yield the best heat transfer performance and enhance the Nusselt number by up to 62% at $Re = 5000$.

Nanoparticles can be added into pure fluid to form nanofluid, which has also been widely applied for the enhancement of heat transfer performance. For instance, Hilo *et al.*[17] performed an experiment to study the nanofluid flow and heat transfer in a channel with BFS at $5000 \leq Re \leq 20\,000$. They found that the Nusselt number increases by up to 11% at 0.05 volume concentration. Abu-Nada[18] numerically studied the heat transfer performance of a channel with a BFS at $Re = 800$ and $Pr = 0.7$, in which a nanofluid is applied. The results show that the best heat transfer efficiency in the recirculation zone mainly depends on the thermophysical properties of the nanofluid and is independent of the Reynolds number. The best performance can be yielded by TiO_2 rather than by other nanoparticles, such as Ag, Cu, Al_2O_3, and CuO.

In some other studies, the above two strategies have been adopted simultaneously. For example, Ma *et al.*[19] carried out a numerical study on multi-walled carbon nanotubes (MWCNT)-Fe_3O_4/water hybrid nanofluid forced convection in a channel with a BFFS ($25 \leq Re \leq 100$), where a vertical stationary baffle is placed on the top wall. They found that the heat transfer is improved when a longer baffle and a higher volume fraction of nanofluid are used.

From the perspective of flow control, the aforementioned approaches are passive flow control (PFC) methods, since they generally rely on changing the geometric configuration or types of fluid. In contrast, active flow control (AFC) can introduce a tunable amount of energy into the ambient flow through actuators. Hence, it is usually more effective and robust for achieving the desired control objectives. Due to the presence of steps, flow separation and reattachment are exhibited, forming recirculation zones. Hence, the flow in the channel with steps is often more complex than that of a bare channel, resulting in more intricate heating or cooling processes. Such intricacies are sometimes further increased by the application of PFC. Therefore, employing AFC is a good option for accurate control of heat transfer characteristics.

Thus far, AFC has been utilized in a few studies where a channel with a BFS is considered. Particularly, Kumar and Vengadesan[20] applied an oscillating fin to enhance the heat transfer in a flow over a BFS at $Re = 400$ and $Pr = 0.71$. They found that heat transfer performance can be enhanced by increasing the velocity or oscillation frequency. Moayedi[21] numerically studied the effects of oscillating injection flow on the nanofluid forced convection heat transfer in a channel with a BFS. They found that by the oscillating injection, the heat transfer performance can be enhanced by around 44%. Kiwan[22] investigated the effects of jet location, angle, and velocity on the fluid flow and heat transfer in a channel with a BFS. It was found that a jet can greatly affect thermo-fluid dynamics. Optimal heat transfer performance is achieved when the jet angle is set at 20°, and when it is 3.1 times the BFS height away from the BFS. Selimefendigil *et al.*[23] applied a rotating cylinder in a BFS channel to alter the nanofluid flow and heat transfer at $50 \leq Re \leq 200$. They found that a rotating circular cylinder with the non-dimensional angular velocities of −4.5 and 1.5 can effectively improve heat transfer. Selimefendigil and Oztop[24] employed carbon-nanotubes/water nanofluid in a channel with a double BFS and rotating tube bundle at $100 \leq Re \leq 500$. A positive linear correlation of the average Nusselt number with volume fraction was identified, and the heat transfer performance can be increased by 52% compared to that of pure water when the volume fraction is 0.02. Furthermore, they found that clockwise rotation is more beneficial to enhancing heat transfer.

Compared to PFC, AFC has been less frequently adopted to improve the heat transfer performance of a channel with BFS, and it has not been employed for the channel with other types of steps. In other words, the effectiveness of AFC in enhancing the heat transfer of a channel with FFS or BFFS remains unknown, and so does how the enhancement can be achieved. This study aims to bridge this gap. Specifically, a channel with BFFS is considered, and a single rigid plate is applied, which can undergo periodic rotation between the two steps in the channel at different frequencies, orientations, and positions. The influences of these factors on the heat transfer performance of the channel are explored systematically.

The remainder of this paper is organized as follows. The problem setup and the numerical method are described in Sec. II. The simulation results are discussed in Sec. III, where the effects of a stationary plate and a rotating plate on the heat transfer performance are discussed and analyzed sequentially. A conclusion is given in Sec. IV.

II. PROBLEM DESCRIPTION AND METHODOLOGY

In this study, a two-dimensional rectangular channel is considered, as shown in Fig. 1. The height of the inlet and the outlet is H_0. One BFS and one FFS of height H_s are inside the channel, and the length of recess between BFS and FFS is L. Herein, the channel acts as a heat sink, utilizing the cooling fluid of temperature T_c, which is injected through the inlet. The cooling fluid takes away the heat produced at the bottom wall between the two steps, where the temperature is fixed at T_h. In addition to the forced convection, the natural convection arising from the buoyance force due to the downward-pointing gravity field is also considered.

To manipulate the heat transfer, a rigid plate of length $l = H_0$ and temperature T_c is placed between the two steps. The plate rotates around one edge, which is located at $x = S$ and $y = D$. Herein, the rotational motion of the plate is prescribed as

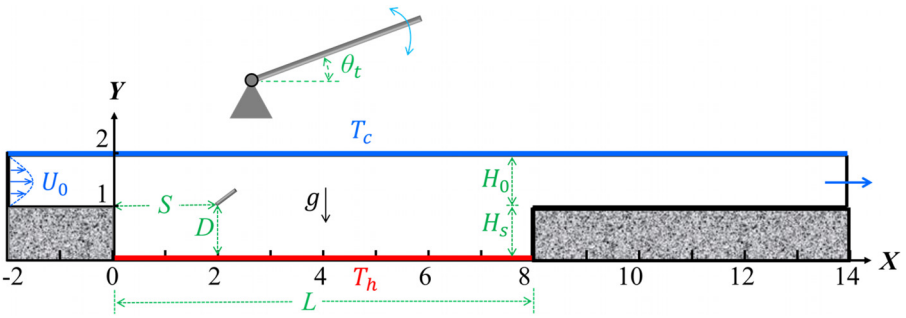

FIG. 1. Schematic of a plate rotating in the channel with a BFS and an FFS of height H_s. Here, U_0 is the mean flow velocity at the inlet. S and D are the horizontal and vertical positions of the plate, respectively. L is the recess length. H_0 is the height of the inlet and the outlet. The wall marked in red denotes the hot wall with temperature T_h that colored in blue represents the cold wall with temperature T_c, and those highlighted in black are insulated.

$$\theta_t = \theta_\alpha \cos(2\pi f_r t) + \theta, \tag{1}$$

where θ is the mean orientation angle, f_r is the rotation frequency, and θ_α is the rotation amplitude, which is fixed at 0.5π in this study.

The above problem is governed by the following equations:

$$\nabla \cdot \boldsymbol{u} = 0, \tag{2}$$

$$\frac{\partial \boldsymbol{u}}{\partial t} + \boldsymbol{u} \cdot \nabla \boldsymbol{u} = -\frac{1}{\rho_0}\nabla p + \nu \nabla^2 \boldsymbol{u} + \boldsymbol{f}, \tag{3}$$

$$\frac{\partial T}{\partial t} + \boldsymbol{u} \cdot \nabla T = \nabla \cdot (\alpha \nabla T), \tag{4}$$

where $\boldsymbol{u}$ is the fluid velocity, p is the pressure, ν is the kinematic viscosity, T is the fluid temperature, α is the thermal diffusivity, ρ_0 is the fluid density, and $\boldsymbol{f}$ is the body force.

When choosing ρ_0, the mean fluid velocity at the inlet (U_0), the height of the inlet and outlet (H_0) and T_h–T_c as repeating variables, the following non-dimensional parameters can be derived $x^* = \frac{x}{H_0}$, $y^* = \frac{y}{H_0}$, $u^* = \frac{u}{U_0}$, $v^* = \frac{v}{U_0}$, $T^* = \frac{T-T_c}{T_h-T_c}$, $t^* = \frac{t}{H_0/U_0}$, $f_r^* = \frac{H_0}{U_0} f_r$, $\nabla^* = H_0 \nabla, p^* = \frac{p}{\rho_0 U_0^2}, \boldsymbol{f}^* = Ri T^*$.

Equation (2)–(4) can be expressed as

$$\nabla \cdot \boldsymbol{u}^* = 0, \tag{5}$$

$$\frac{\partial \boldsymbol{u}^*}{\partial t^*} + \boldsymbol{u}^* \cdot \nabla^* \boldsymbol{u}^* = -\nabla^* p^* + \frac{1}{\mathrm{Re}} \nabla^{*2} \boldsymbol{u}^* + Ri T^*, \tag{6}$$

$$\frac{\partial T^*}{\partial t^*} + \boldsymbol{u}^* \cdot \nabla^* T^* = \frac{1}{Re \cdot Pr} \nabla^{*2} T^*, \tag{7}$$

where Re is the Reynolds number, Ri is the Richardson number, and Pr is the Prandtl number, which can be expressed as

$$Re = \frac{U_0 H_0}{\nu}, \tag{8}$$

$$Ri = \frac{g\beta(T_h - T_c)H_0}{{U_0}^2}, \tag{9}$$

$$Pr = \frac{\nu}{\alpha}, \tag{10}$$

where g is the gravitational acceleration and β is the thermal expansion coefficient. For simplicity, the symbol "$*$" is dropped henceforth.

Herein, three Nusselt numbers are used to quantify the heat transfer performance over the hot bottom wall, i.e., instantaneous local Nusselt number (Nu_{loc}), spatial-averaged Nusselt number (Nu_{avg}), and time- and spatial-averaged Nusselt number (Nu_{mean}). They are defined as[25]

$$Nu_{loc}(x,t) = \left.\frac{\partial T(x,\, y,\, t)}{\partial y}\right|_{y=0}, \tag{11}$$

$$Nu_{avg}(t) = \frac{1}{L} \times \int Nu_{loc}(x,\, t)dx, \tag{12}$$

$$Nu_{mean} = \frac{1}{L \times \Delta t} \int\int Nu_{loc}(x,\, t)dxdt, \tag{13}$$

where Δt is the time interval for time-averaging.

The lattice Boltzmann method (LBM)[26–28] is used to solve the above thermo-fluid problem, and the immersed boundary method[29] is employed to solve the interplay between the flow and structure dynamics and to impose the no-slip boundary condition as well as the Dirichlet boundary condition for the temperature. The adopted solvers have been validated and extensively applied in our previous works.[30–32,39]

In this study, the no-slip boundary condition is imposed on the plate surface and the inner walls of the channel. The velocity boundary condition is imposed at the inlet where a parabolic profile is assumed,[33] while a constant pressure is set at the outlet,[34] as shown in Fig. 1. The Dirichlet boundary condition for the temperature is imposed on the inlet, top and bottom walls as well as on the plate surface, whereas the adiabatic boundary condition is applied on the other boundaries.[35]

Herein, uniform mesh is implemented. To ensure that the numerical results are independent of the mesh resolution, four cases are selected for the convergence test when $S = L/4$, $f_r = 0.3$ and $\theta = 0.5\pi$, i.e., the cases with $H_0 = 20\Delta x$, $40\Delta x$, $80\Delta x$, and $160\Delta x$, as shown in Fig. 2(a). It is seen that the time history of Nu_{avg} in the case with $H_0 = 80\Delta x$ is sufficiently close to that in the case with $H_0 = 160\Delta x$, meaning that the mesh with $H_0 = 80\Delta x$ is fine enough to yield converged results. Therefore, $H_0 = 80\Delta x$ is adopted throughout this study, and the mesh around the plate is illustrated in Fig. 2(b).

For simplicity, Ri and Pr are fixed at 1 and 0.7, respectively. Re is set at 100,[13,21,36,37] unless otherwise stated. The geometric configuration of the channel is given in Fig. 1 and remains unchanged throughout this study. The plate length is set as $l = 0.5$, i.e., it is half of the height of the inlet and outlet. The vertical location of the pivot edge of the plate is selected as $D = 1$. Under this condition, the heat transfer performance depends on the non-dimensional rotating frequency (f_r), the orientation angle (θ), and the horizontal location of the plate (S).

In the following, two scenarios are considered. In one scenario, the plate remains stationary, corresponding to $f_r = 0$, and in the other scenario the rotating-plate cases, where f_r is selected as $0.01 \leq f_r \leq 1$, covering a sufficiently wide range of rotation frequency. In these two

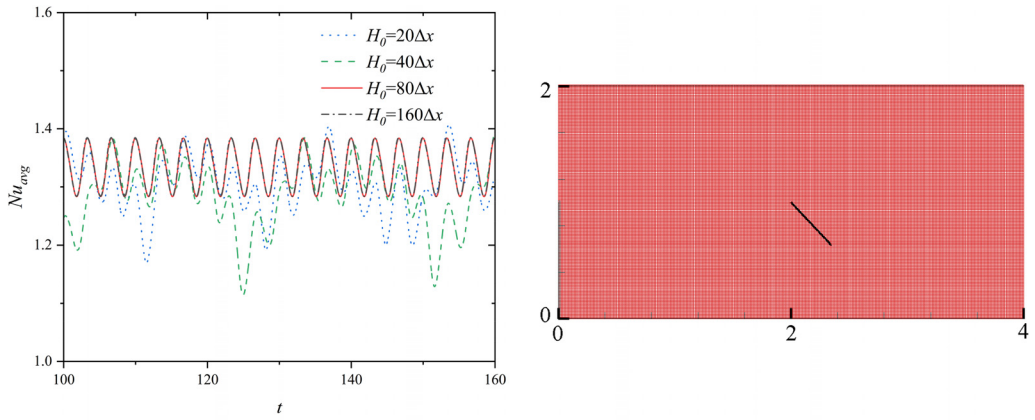

FIG. 2. (a) Time history of Nu_{avg} in the cases with $S = L/4$, $f_r = 0.3$ and $\theta = 0.5\pi$, when $H_0 = 20\Delta x$, $40\Delta x$, $80\Delta x$, and $160\Delta x$ and (b) mesh near the plate for $H_0 = 80\Delta x$.

scenarios, four θ values are adopted, and S is chosen as $L/4$, $L/2$, and $3L/4$, as given in Table I. The influences of the stationary plate on the heat transfer are discussed first to assess the performance of PFC. After that, the effects of the rotating plate are discussed to evaluate the performance of AFC.

III. RESULTS AND DISCUSSION

A. PFC using a stationary plate

Figure 3 shows that compared to that in the case without a plate, the time- and spatial-averaged Nusselt number over the bottom wall between the two steps (Nu_{mean}) is enhanced in all cases with a plate. This means that the plate can improve the heat transfer performance of the channel, regardless of its horizontal location (S) and orientation angle (θ). However, the improvement in Nu_{mean} greatly depends on these two parameters. Specifically, Nu_{mean} is larger when the plate is placed closer to the BFS, i.e., when $S = L/4$ and $L/2$. In addition, Nu_{mean} usually approaches the maximum when $\theta = 0.5\pi$. When $S = L/4$ and $\theta = 0.5\pi$, $Nu_{mean} = 1.27$, which is 144% larger than $Nu_{avg} = 0.52$ in the case without a plate.

To reveal how the heat transfer is improved by the stationary plate, in the following, the cases with $S = L/4$ are discussed first, and then the discussion is broadened to include the cases with other S.

In the case without a plate, the instantaneous spatial-averaged Nusselt number (Nu_{avg}) remains constant, as shown in Fig. 4(a). This is attributed to that the flow is steady, and the temperature, vorticity, and velocity magnitude contours are independent of time, as shown in Figs. 5(a1)–5(a3). In this case, the local Nusselt number (Nu_{loc}) approaches the maximum at around $x = 6$, as shown in Fig. 4(b), where the temperature gradient in the vertical direction is the highest, as shown in Fig. 5(a1). This location corresponds to where the flow in the recirculation region reattaches to the bottom wall, as shown in Fig. 5(a3).

When a plate is placed at $S = L/4$, Nu_{mean} is larger than that in the case without a plate regardless of θ. The maximum enhancement is obtained when the plate is oriented upward, i.e., $\theta = 0.5\pi$. Additionally, when $\theta = 0$ and 0.5π, Nu_{avg} varies periodically, indicating that the flow is unsteady in these two cases. The spectral analysis shows that the dominant frequency of Nu_{avg} is 0.1 and 0.25 in the cases with $\theta = 0$ and 0.5π, respectively, as shown in Fig. 4(c). These frequencies are correlated with the variation in the thermo-fluid dynamics of the system, and they are equal to the natural vortex shedding frequency (f_n). Note that although the instability does not set in when $\theta = \pi$, and 1.5π, it can be triggered if the Reynolds number (Re) is slightly raised above 100, i.e., at around 120 and 110 for $\theta = \pi$, and 1.5π, respectively.

TABLE I. Values of the key non-dimensional parameters.

Parameter	Values
f_r	0 and 0.01 to 1
θ	0, 0.5π, π, 1.5π
S	$L/4$, $L/2$, $3L/4$

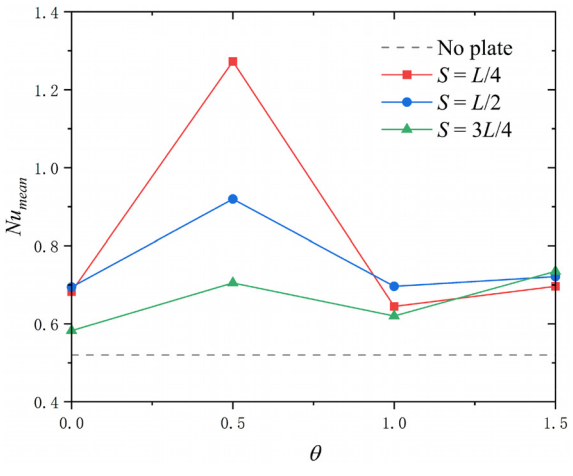

FIG. 3. Time- and spatial-averaged Nusselt number (Nu_{mean}) in the case without a plate (denoted by the dashed line) and those with a stationary plate at different θ and S (denoted by the solid lines with solid symbols).

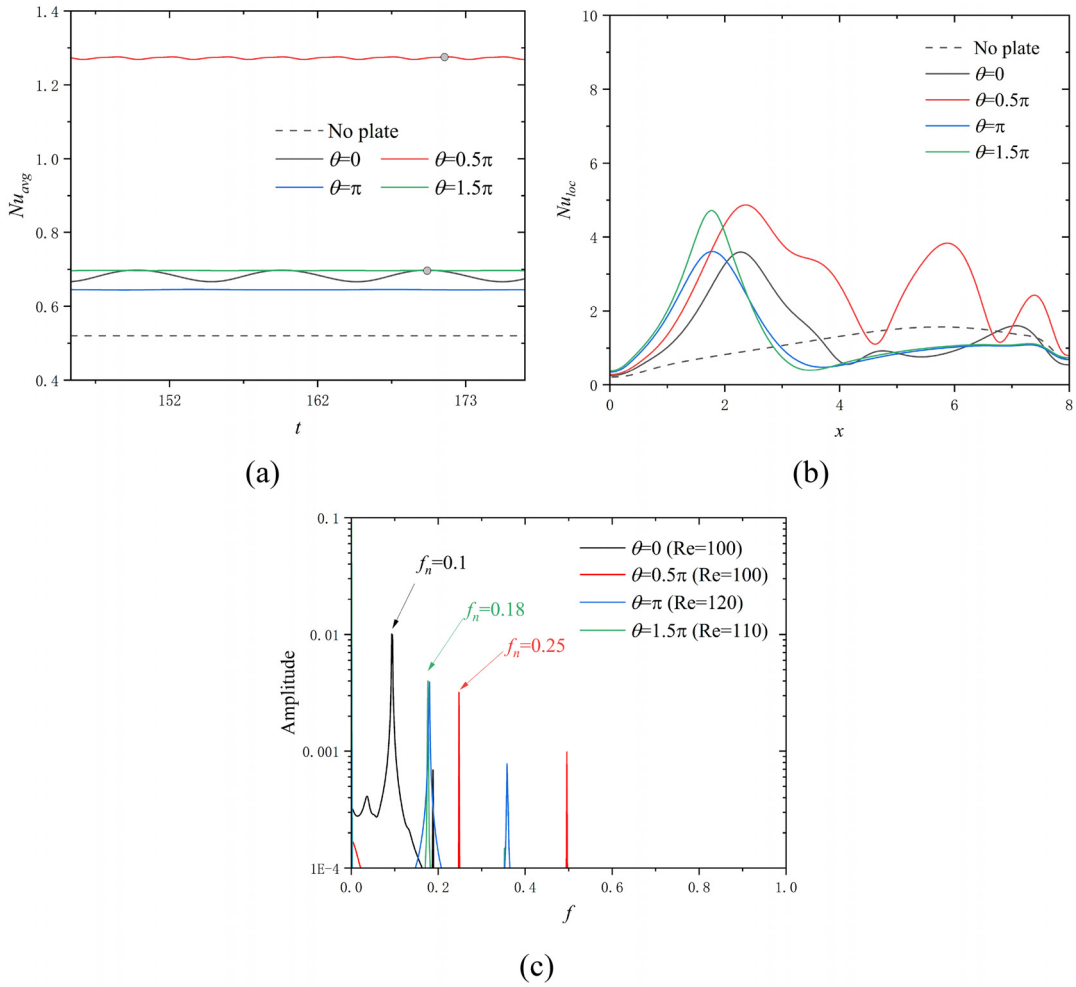

FIG. 4. Time history of the spatial-averaged Nusselt number (Nu_{avg}) (a) and the local Nusselt number (Nu_{loc}) along the bottom wall (b) in the case without a plate and the cases with $\theta = 0$, 0.5π, π, and 1.5π when $S = L/4$. Frequency spectra of Nu_{avg} in the cases with $\theta = 0$, 0.5π, π, and 1.5π at the Reynolds number $Re = 100$, 110, or 120 (c). The solid symbols on the Nu_{avg} curves in panel (a) denote the instants selected for plotting the corresponding Nu_{loc} curves in panel (b).

In both cases, the natural frequency is $f_n = 0.18$, which is roughly twice that in the case with $\theta = 0$, as shown in Fig. 4(c).

Compared to that in the case without a plate, Nu_{loc} in all cases with $S = L/4$ is mainly enhanced near the location where it is placed, i.e., at $x = L/4$, as shown in Fig. 4(b). In these cases, the cooling flow from the inlet is redirected by the plate toward the bottom wall, corresponding to the shortened recirculation in the downstream of the BFS ($0 < x < 2$), as shown in the third column of Fig. 5. Under this condition, the temperature gradient is enhanced under the plate, augmenting Nu_{loc} at around $x = 2$. When the plate is oriented upward or downward, i.e., $\theta = 0.5\pi$ and 1.5π, such influences are more pronounced, as shown in Fig. 5, and Nu_{loc} at around $x = 2$ in the cases with $\theta = 0.5\pi$ and 1.5π is obviously higher than that in those with $\theta = 0$ and π. Note that when $\theta = 0$ and 0.5π, the flow is unsteady, and Nu_{loc} is time-dependent. Under this circumstance, the instants at which Nu_{avg} approaches the maximum, denoted by the solid symbols in Fig. 4(a), are selected for plotting the Nu_{loc} along the bottom wall in Fig. 4(b). This convention is adopted throughout this study, unless otherwise stated.

Furthermore, in the cases with $\theta = 0$ and 0.5π where the flow is unsteady, the enhancement can also be achieved in the downstream to different extents, as shown in Fig. 4(b). When $\theta = 0.5\pi$, the flow directly separates from the lower and upper edges of the plate, producing alternatively shed vortices at $f_n = 0.25$, as shown in Fig. 5(c2). These vortices greatly enhance the flow and heat transport as well as the mixing between the two steps, especially in the vertical direction. Under this condition, two cold plumes are exhibited at around $x = 6$ and 7.5, respectively [see Fig. 5(c1)], and the velocity magnitude near the bottom wall is enhanced [see Fig. 5(c3)], indicating stronger forced convection. As such, the temperature gradient in the downstream is significantly amplified near $x = 6$ and 7.5. By contrast, although the flow instability also sets in when $\theta = 0$, the plate is aligned in the streamwise direction and produces a long shear layer, which starts to flap periodically at $f_n = 0.1$ only near the upstream of the FFS and

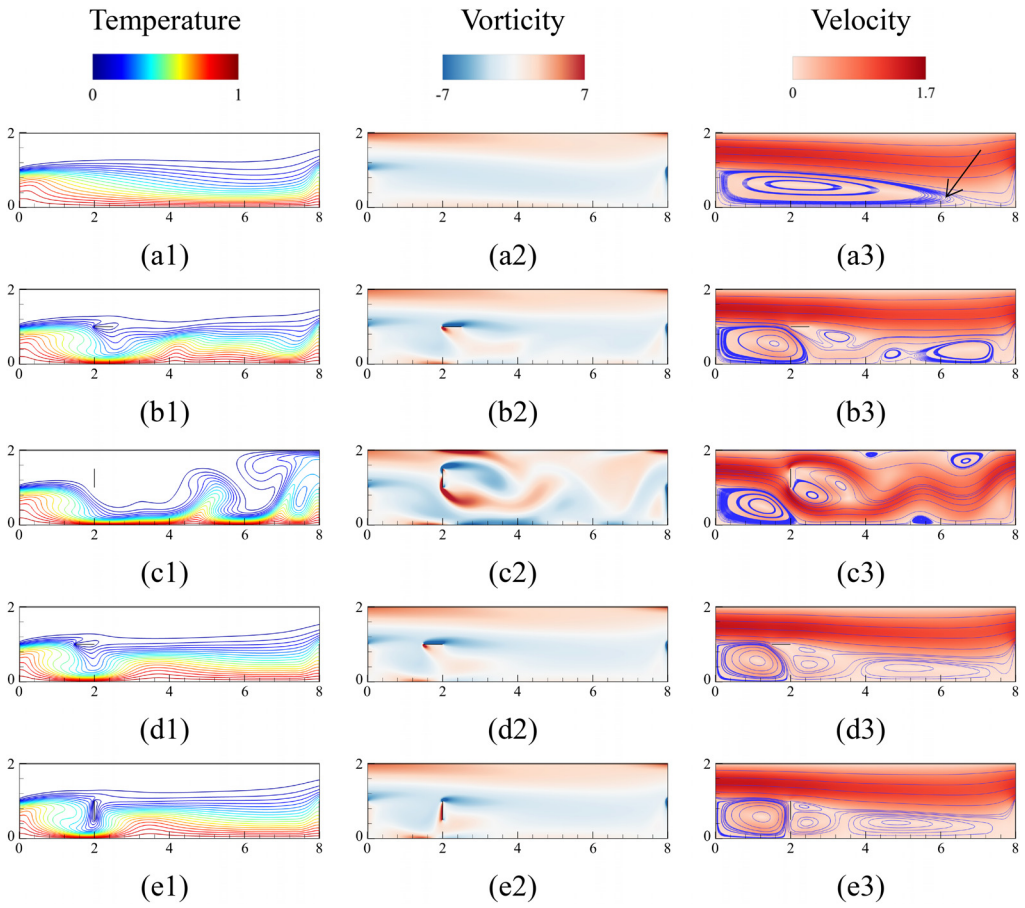

FIG. 5. Isothermal lines (the first column), vorticity contour (the second column), and streamlines and velocity contour (the third column) for the case without a plate (a1)–(a3) and for the stationary-plate cases with $S = L/4$ when $\theta = 0$ (b1)–(b3), $\theta = 0.5\pi$ (c1)–(c3), $\theta = \pi$ (d1)–(d3), and $\theta = 1.5\pi$ (e1)–(e3). Note that only the region between the two steps in the channel is showcased to provide a more concise and focused perspective. The color bars in this figure are also applied to other similar figures.

causes a considerably weak unsteadiness in the flow. Under this circumstance, Nu_{loc} is slightly enhanced only at $x \approx 7$, as shown in Fig. 4(b).

The aforementioned analysis is generally applicable to the cases with $S = L/2$ and $3L/4$. For instance, when $\theta = 0.5\pi$, Nu_{avg} can also be enhanced by the plate in the cases with $S = L/2$ and $3\,L/4$, as shown in Fig. 6(a). The enhancement is mainly achieved in the region between the plate and the FFS, similar to that in the case with $S = L/4$ and $\theta = 0.5\pi$, as shown in Fig. 6(b). Despite these similarities, the influences of S on the heat transfer are still remarkable, as it determines the extent to which and the location where Nu_{loc} can be enhanced. Specifically, the redirection effects of the plate on the incoming cooling flow turn less significant with S, as evidenced by the fact that at a larger S, the strength of the vortex shed from the lower edge of the plate is weaker, and the velocity magnitude of the flow circumnavigating this edge and flowing toward the bottom wall is smaller, as shown in Fig. 7 and the third row of Fig. 5. As such, the maximum Nu_{loc} decreases with S, as shown in Fig. 6(b). Furthermore, considering that the plate mainly alters the flow and heat transport between it and the FFS, it is not surprising to see that the improvement is less significant at a larger S, as shown in Fig. 6(a).

The above discussion demonstrates that the heat transfer performance in the channel with the BFFS can be enhanced by a stationary plate from two aspects. One is the local enhancement of Nu_{loc} near the plate due to the cooling flow redirected toward the bottom wall. The other is the improvement in Nu_{loc} in the wake region, resulting from that the plate could trigger flow instability, cause vortex shedding, and eventually enhance fluid and heat transport.

B. AFC using a rotating plate

1. Overview

Figure 8 shows the variation in the time- and spatial-averaged Nusselt number over the bottom wall between the two steps (Nu_{mean}) with the plate orientation angle (θ) at different rotation frequencies (f_r), and horizontal locations (S). When compared to that in the case without a plate, Nu_{mean} is enhanced in all cases with the plate no matter whether it is stationary or not, meaning that as long as a rigid plate

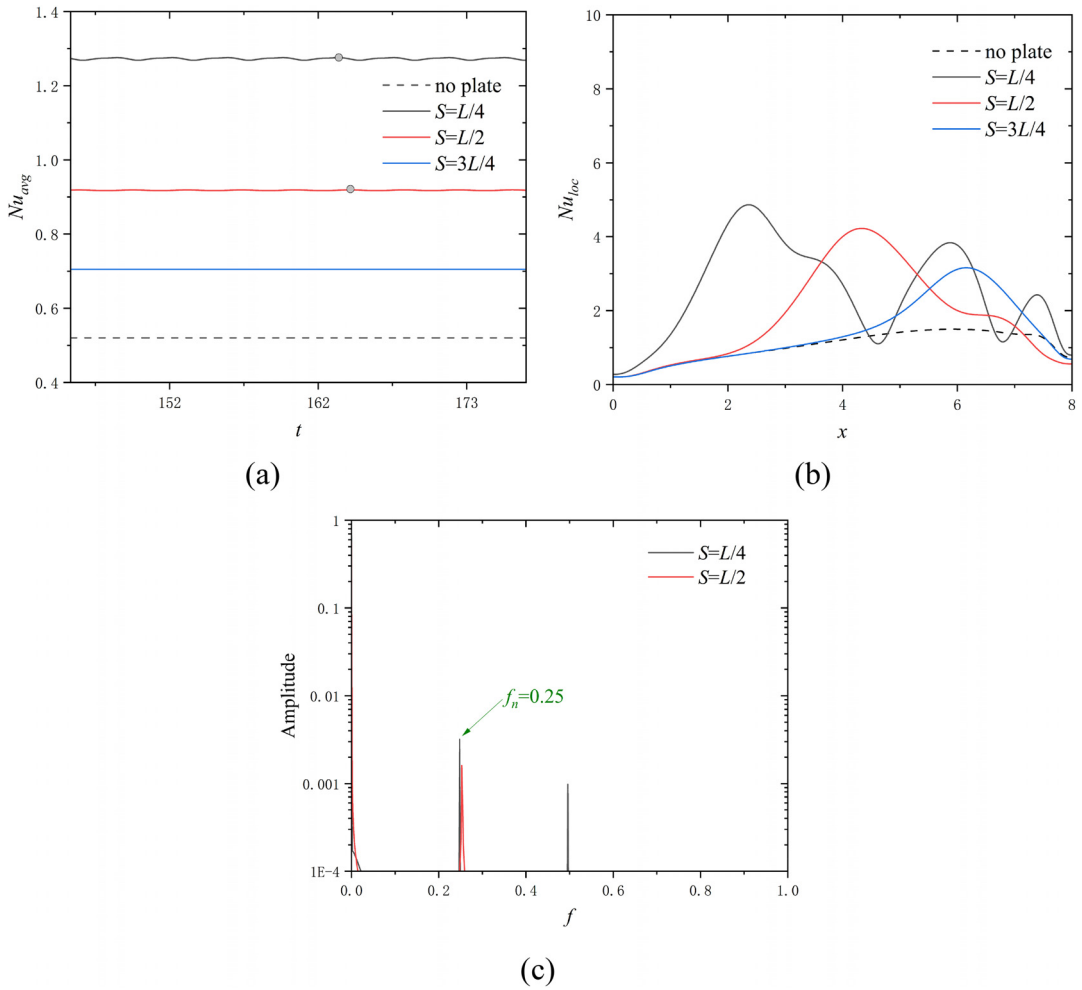

FIG. 6. Time history of the spatial-averaged Nusselt number (Nu_{avg}) (a) and the local Nusselt number (Nu_{loc}) along the bottom wall (b) in the case without a plate and the cases with $S = L/4$, $L/2$, and $3L/4$ when $\theta = 0.5\pi$. Frequency spectra of Nu_{avg} in the cases with $S = L/4$ and $L/2$ (c). The solid symbols on the curves in panel (a) denote the instants selected for plotting the corresponding curves in panel (b).

is placed between the two steps, the heat transfer performance can be improved. If compared with the stationary-plate case, it is found that the amelioration of Nu_{mean} can be achieved by the rotating plate at all S, while the specific improvement depends on θ and f.

In particular, when $S = L/4$, Nu_{mean} can be enhanced at all f_r in the cases with $\theta = 0$, π, and 1.5π, compared to that in the stationary-plate case. In these cases, the maximum Nu_{avg} can be achieved at $f_r = 0.1$, whereas $f_r = 0.01$ and 1 yield the minimum Nu_{mean}, as shown in Fig. 8(a). In contrast, the enhancement can be achieved only at $f_r = 0.3$ and 1 when $\theta = 0.5\pi$, while Nu_{mean} at other f_r is smaller than that in the stationary-plate case. At all f_r except $f_r = 0.1$, Nu_{mean} approaches the maximum when $\theta = 0.5\pi$, similarly to the stationary-plate case, whereas at $f_r = 0.1$, Nu_{mean} approaches the minimum when $\theta = 0.5\pi$. Among all cases with $S = L/4$, Nu_{mean} approaches the maximum 1.37 at $\theta = 0.5\pi$, and $f_r = 1$.

When $S = L/2$, the variation trends of Nu_{mean} with f_r and θ are similar to those when $S = L/4$, as shown in Figs. 8(a) and 8(b), while the values of Nu_{mean} are generally smaller. This mainly results from the fact that the region where the flow can be altered shrinks with S. For the same reason, Nu_{mean} is roughly further reduced when S increases from $L/2$ to $3L/4$, as shown in Fig. 8(c). As such, the enhancement of the heat transfer performance is the weakest when $S = 3L/4$.

Figure 8 demonstrates that Nu_{mean} can be influenced evidently by all three parameters, i.e., S, θ, and f_r. To reveal their effects, several cases are selected and further discussed in Secs. III B 2–III B 5. Specifically, some cases with $S = L/4$ are considered first to reveal the influences of θ and f, and then a few cases with other S are discussed to unveil the effects of S.

2. Effects of f_r when $\theta = 0.5\pi$

When the orientation angle $\theta = 0.5\pi$, compared to that in the stationary-plate case, the instantaneous spatial-averaged Nusselt number (Nu_{avg}) can be enhanced in the case with the rotation frequency

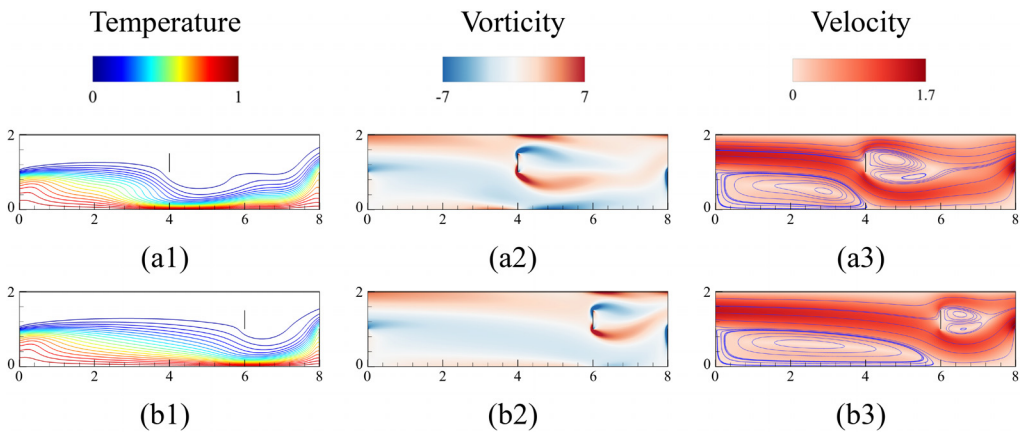

FIG. 7. Isothermal lines (first column), vorticity contour (second column), and streamlines and velocity contour (third column) of the case with $S = L/2$ (a1)–(a3) and $S = 3L/4$ (b1)–(b3) when $\theta = 0.5\pi$.

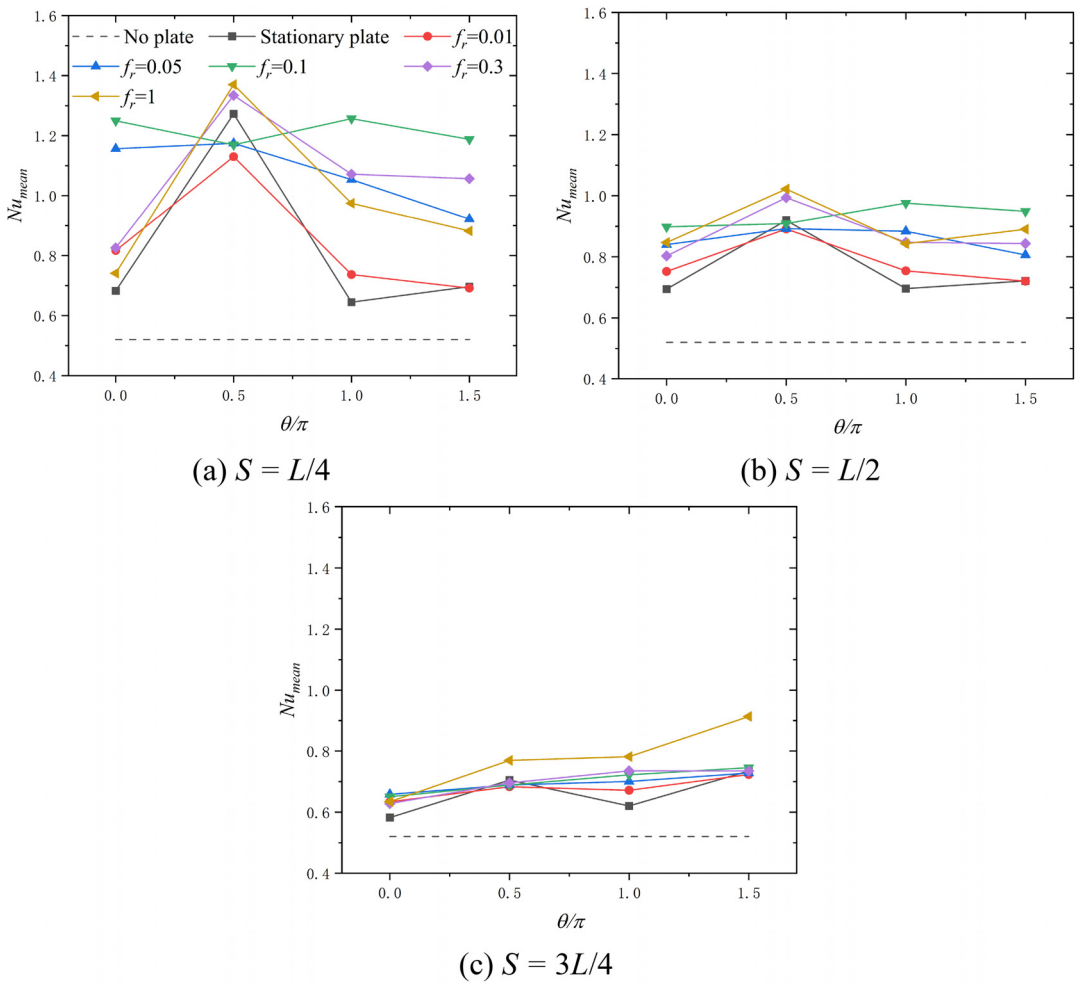

FIG. 8. Time- and spatial-averaged Nusselt number (Nu_{mean}) in the case without a plate (denoted by the dashed line), those with a stationary plate at different θ and S (denoted by the dark solid lines with dark square symbols), and those with a rotating plate at different f_r, θ, and S (denoted by other solid lines with other slid symbols).

$f_r = 0.3$, as shown in Fig. 9(a). The enhancement is achieved mainly in the wake roughly from $x = 4$ to 8, if comparing the local Nusselt number (Nu_{loc}) in these two cases, as shown in Fig. 9(b). Specifically, Nu_{loc} approaches larger local maxima at around $x = 5$ and 7 in the case with $f_r = 0.3$ than those in the stationary-plate case, respectively. Such an enhancement arises from the fact that the rotating plate produces stronger and more compact vortices in the wake and amplifies the velocity magnitude near the bottom wall, as shown in the first and fourth rows of Fig. 10. These augmentations are associated with stronger mixing and transport processes and accompanied by the presence of two stronger cold plumes impinging more intensely on the bottom wall at around $x = 5$ and 7, yielding higher temperature gradients and larger Nu_{loc}.

It is not surprising to see that the heat transfer performance is enhanced by the plate rotating at $f_r = 0.3$, when recalling that the natural vortex shedding frequency $f_n = 0.25$ in the stationary-plate case (see Sec. III A). As $f_r = 0.3$ is close to $f_n = 0.25$, an interesting physical phenomenon occurs due to the nonlinear characteristics of the thermo-fluid system, i.e., vortex synchronization.[38,39] In such a case, the vortex shedding frequency can be entrained to the frequency of the external forcing, i.e., the rotation frequency f_r in this study [see Fig. 9(c)]. When this happens, the vortex strength could be enhanced, improving the heat transfer performance. The enhancement is expected to be larger as the external forcing frequency is closer to f_n, as when these two frequencies are equal, resonance occurs. This point can be further corroborated by the fact that Nu_{avg} for $f_r = 0.25$ is larger than that for $f_r = 0.3$, as shown in Fig. 9(a). For $f_r = 0.25$, $Nu_{mean} = 1.39$ is higher than that for all the other f_r considered in this study.

In the case with $f_r = 1$, Nu_{avg} also remains larger than that in the stationary-plate case, but it varies chaotically and corresponds to a non-periodic flow, as shown in Fig. 9(a). Although the vortex synchronization does not occur in this case, larger vortices and cold plumes between the plate and the FFS are still exhibited, and so is the stronger

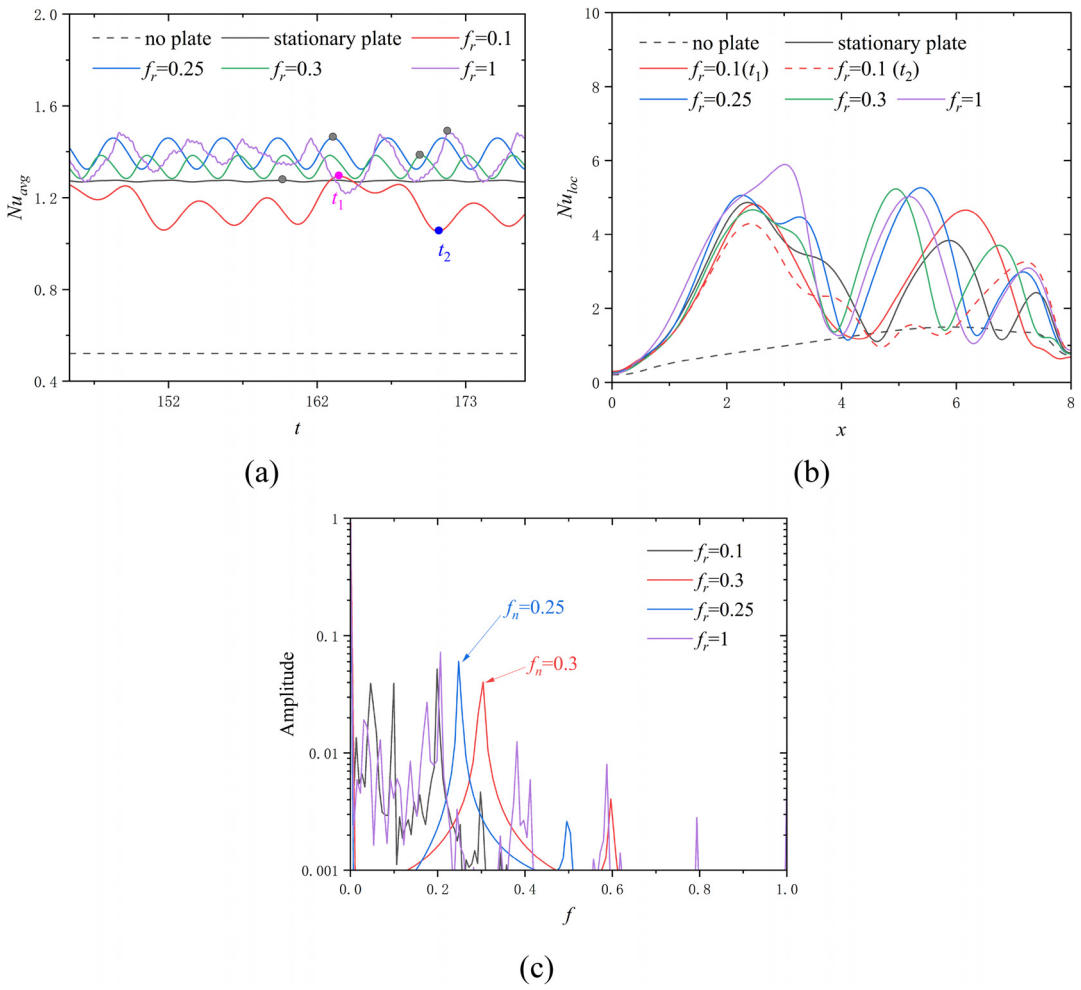

FIG. 9. Time history of the spatial-averaged Nusselt number (Nu_{avg}) (a) and the local Nusselt number (Nu_{loc}) along the bottom wall (b) in the case without a plate, with a stationary plate, and with a rotating plate for which $f_r = 0.1$, 0.25, 0.3, and 1 when $\theta = 0.5\pi$ and $S = L/4$. Frequency spectra of Nu_{avg} in the cases with $f_r = 0.1$, 0.25, 0.3, and 1 (c). The solid symbols on the curves in panel (a) denote the instants selected for plotting the corresponding curves in panel (b).

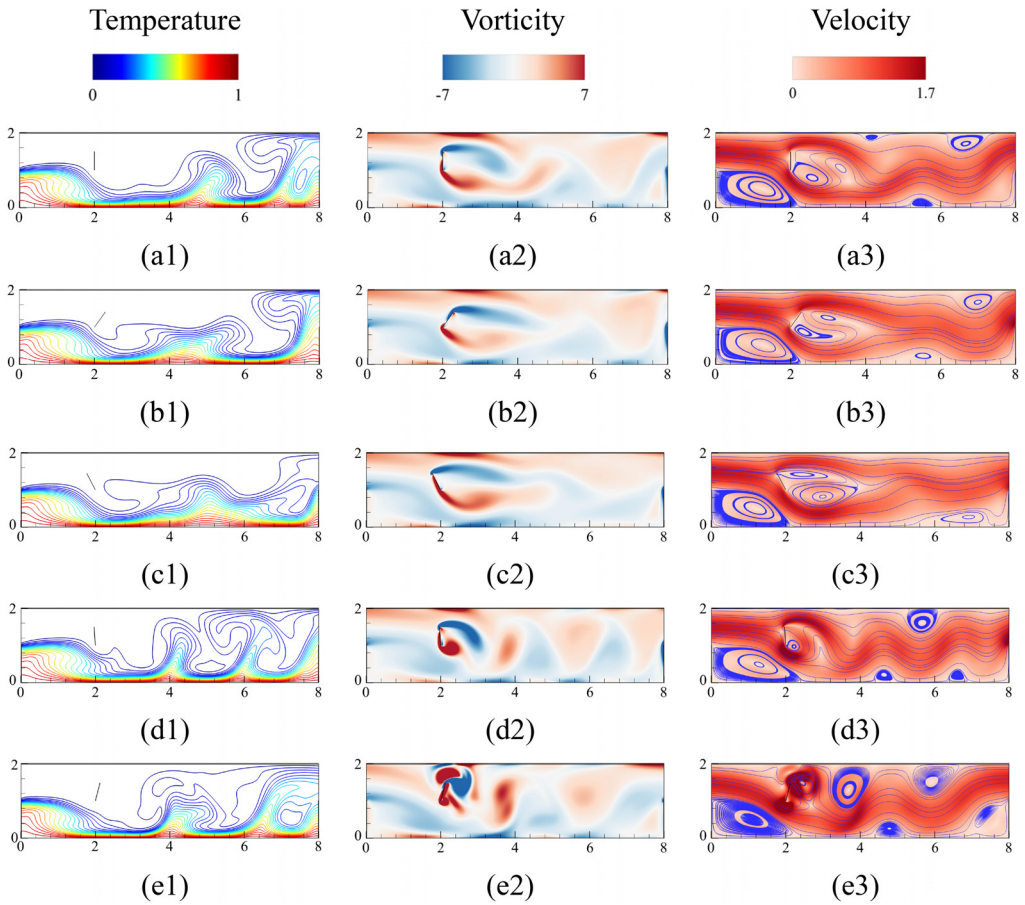

FIG. 10. Isothermal lines (the first column), vorticity contour (the second column), and streamlines and velocity contour (the third column) for the stationary-plate case with (a1)–(a3) when $S = L/4$ and $\theta = 0.5\pi$, and for the rotating-plate case with $f_r = 0.1$ at $t = t_1$ (b1)–(b3), $f_r = 0.1$ at $t = t_2$ (c1)–(c3), $f_r = 0.3$ (d1)–(d3), and $f_r = 1$ (e1)–(e3).

flow near the bottom wall, as shown in the last row of Fig. 10. In this scenario, higher Nu_{loc} can also be attained at around $x = 3$, 5, and 7, as shown in Fig. 9(b), similarly to the case with $f_r = 0.3$.

When $f_r = 0.1$, the variation in Nu_{avg} is also non-periodic, as shown in Fig. 9(a). Unlike the cases with $f_r = 0.3$ and 1, Nu_{avg} is only occasionally comparable to that in the stationary-plate case, such as at $t = 164$, while in most time, Nu_{avg} is smaller. Therefore, the heat transfer performance is worse in the case with $f_r = 0.1$. To elucidate the reasons, two different instants, i.e., $t = 164$ and 171, are selected, which correspond to the maximum and minimum of Nu_{avg} over a long time interval, respectively. At $t = 164$, Nu_{loc} is diminished at around $x = 4$ and 8, as shown in Fig. 9(b) but is enhanced at around $x = 6.2$, due to the presence of the stronger cold plume and augmented velocity magnitude roughly at $6 < x < 7$, as shown in the first and second row of Fig. 10. As a result, Nu_{avg} is roughly the same as those in the cases with the stationary plate and $f_r = 0.1$ at $t = 164$. In contrast, at $t = 171$, the cold plume and velocity magnitude in the wake are weaker than those at $t = 164$, as shown in the second and third row of Fig. 10. As such, Nu_{avg} is much smaller at $t = 171$, as shown in Fig. 9(b).

3. Effects of f_r when $\theta = 0$, π, and 1.5π

When the orientation angle $\theta = 0$, the maximum enhancement of the time- and spatial-averaged Nusselt number over the bottom wall between the two steps (Nu_{mean}) is achieved when the rotation frequency $f_r = 0.1$, compared to that in the stationary-plate case with the same θ, as shown in Fig. 8(a). The instantaneous spatial-averaged Nusselt number (Nu_{avg}) in this case is greatly enhanced and its oscillation amplitude also increases, as shown in Fig. 11(a). The improvement is mainly achieved between the rotation plate and the FFS, i.e., $2 < x < 8$, as shown in Fig. 11(b). Specifically, near $x = 2$, the local Nusselt number (Nu_{loc}) in the case with $f_r = 0.1$ is greater than that in the stationary-plate case. This stems from the fact that the rotating motion causes a stronger flow flowing toward the bottom wall near $x = 2$, which is accompanied by a stronger impingement of a cold plume on the wall, resulting in a higher Nu_{loc}. Furthermore, the rotating plate produces strong and large vortices at $4 < x < 8$, which enhance the flow and heat transport in the wake and induce a strong cold plume near $x = 6$. As such, Nu_{loc} is augmented in the wake when $f_r = 0.1$ compared to that when the plate is stationary and the flow remains roughly steady in a large portion of the wake. It is expected to

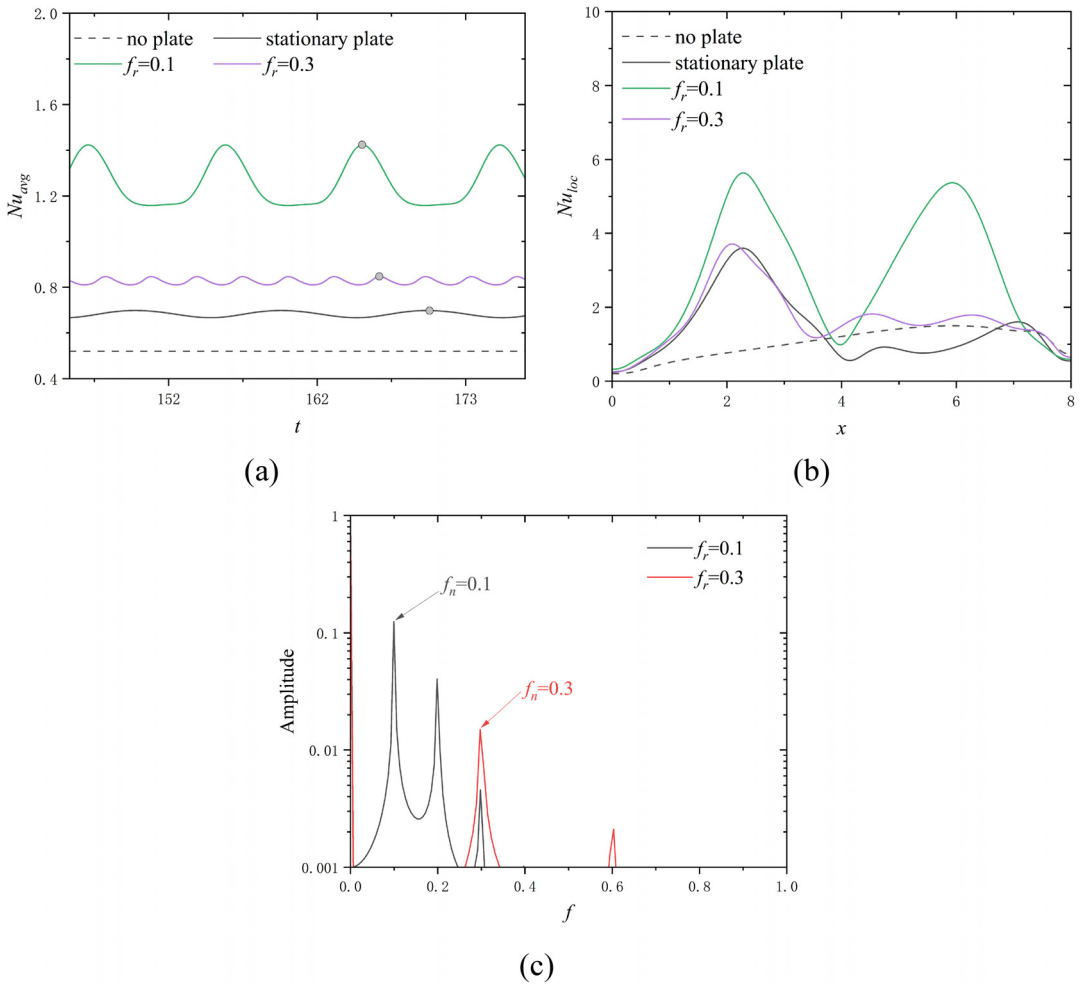

FIG. 11. Time history of the spatial-averaged Nusselt number (Nu_{avg}) (a) and the local Nusselt number (Nu_{loc}) along the bottom wall (b) in the case without a plate, with a stationary plate, and with a rotating plate for which $f_r = 0.1$ and 0.3 when $\theta = 0$ and $S = L/4$. Frequency spectra of Nu_{avg} in the cases with $f_r = 0.1$ and 0.3 (c). The solid symbols on the curves in panel (a) denote the instants selected for plotting the corresponding curves in panel (b).

achieve such an enhancement, if recalling that the instability sets in at $f_n = 0.1$ when the plate is stationary. Thus, $f_r = f_n$ yields the resonance. This is similar to that discussed in Sec. III B 2, where the plate rotating at $f_r = 0.25$ can induce resonance and maximize Nu_{loc} when $\theta = 0.5\pi$.

In contrast, the enhancement is less significant in the cases with other f. Taking the case with $f_r = 0.3$ as an example, even though the vortex shedding frequency (f_v) is attracted to f_r and the vortex synchronization occurs in this case, less improvement in Nu_{mean} and Nu_{avg} is attained compared to that in the case with $f_r = 0.1$, as shown in Figs. 11(a) and 11(c). This results from that Nu_{loc} can only be slightly enhanced at around $4 < x < 7$, as shown in Fig. 11(b). The less considerable enhancement is attributed to the fact that the vortices produced by the rotating plate are smaller and mainly located on the channel centerline, as shown in Fig. 12(c2). As such, the flow and heat transport near the wall cannot be significantly altered, as evidenced by the lower velocity magnitude near the bottom wall, as shown in Fig. 12(c3). Under this circumstance, the cold plumes are much weaker in this case than those in the case with $f_r = 0.1$, and the improvement is discounted.

This analysis reveals that if f_r is not sufficiently close to f_n, a significant improvement cannot be achieved despite the occurrence of vortex synchronization. In other words, to enhance the heat transfer performance, it is essential to set f_r close to f_n as much as possible to trigger the resonance.

In the case with $\theta = 1.5\pi$, the maximum enhancement is achieved when $f_r = 0.1$, compared to the corresponding stationary-plate case. Although the instability does not set in and the flow is steady when $\theta = 1.5\pi$ and the plate is stationary, it can be triggered if the Reynolds number (Re) is slightly increased from 100 to 110, for which the natural vortex shedding frequency $f_n = 0.18$. According to the analysis in Secs. III B 1 and III B 2, the plate that rotates at $f_r = 0.18$ can yield the most significant improvement at $Re = 110$ due to resonance, and f_r which is close to f_n is expected to cause considerable enhancement through vortex synchronization. This can be evidenced by the fact that

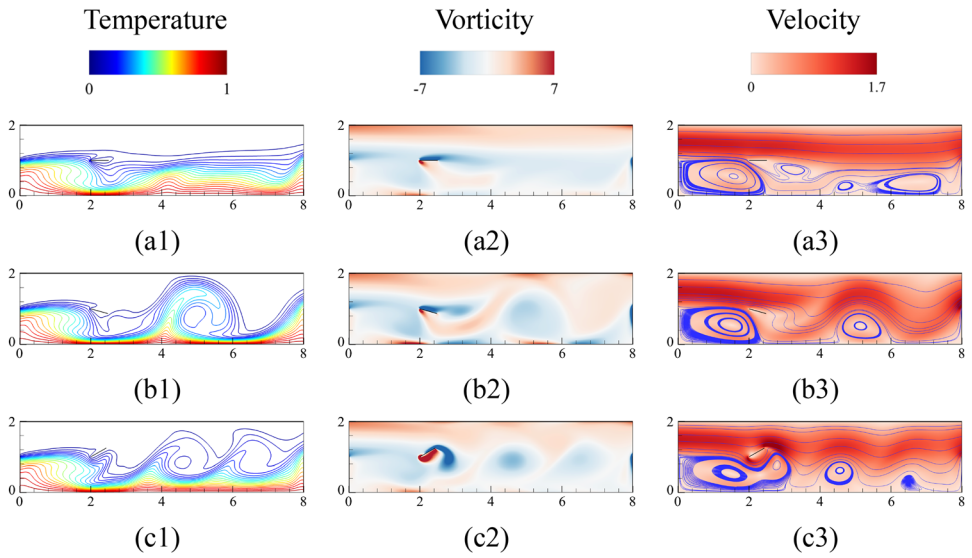

FIG. 12. Isothermal lines (the first column), vorticity contour (the second column), and streamlines and velocity contour (the third column) for the case with a stationary plate with $S = L/4$ and $\theta = 0$ (a1)–(a3) and for the rotating-plate case with $f_r = 0.1$ (b1)–(b3) and $f_r = 0.3$ (c1)–(c3).

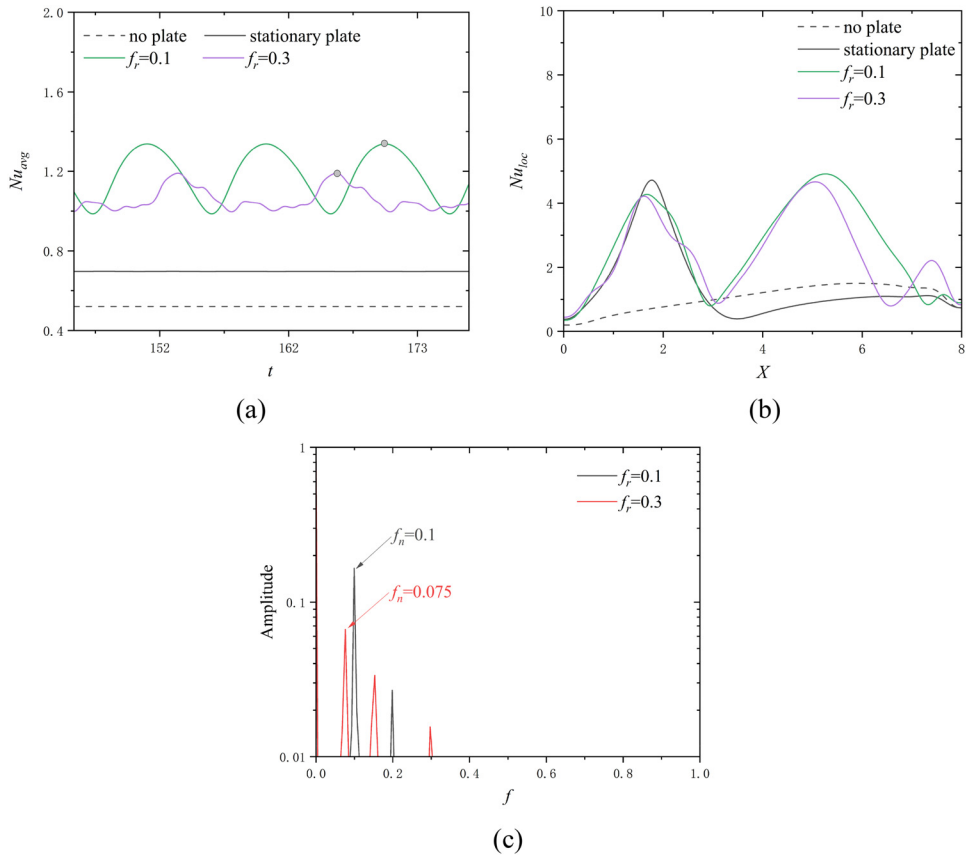

FIG. 13. Time history of the spatial-averaged Nusselt number (Nu_{avg}) (a) and the local Nusselt number (Nu_{loc}) along the bottom wall (b) in the case without a plate, with a stationary plate, and with a rotating plate for which $f_r = 0.1$ and 0.3 when $\theta = 1.5\pi$ and $S = L/4$. Frequency spectra of Nu_{avg} in the cases with $f_r = 0.1$ and 0.3 (c). The solid symbols on the curves in panel (a) denote the instants selected for plotting the corresponding curves in panel (b).

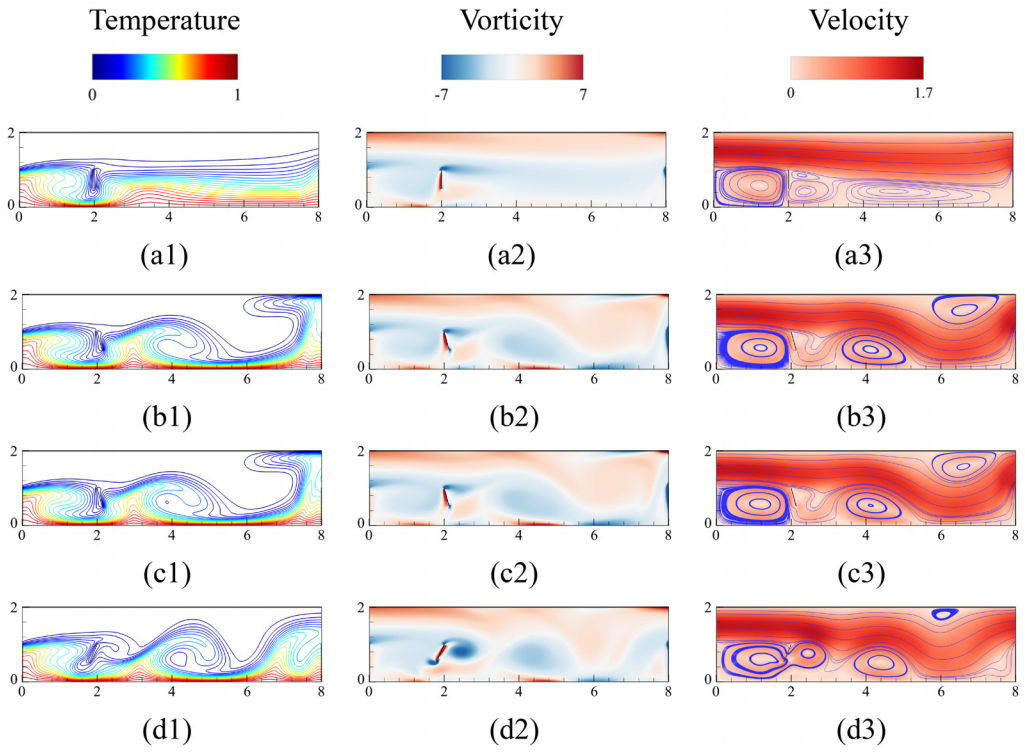

FIG. 14. Isothermal lines (the first column), vorticity contour (the second column), and streamlines and velocity contour (the third column) for the case with a stationary plate (a1)–(a3) when $S = L/4$ and $\theta = 1.5\pi$, for the rotating-plate case with $f_r = 0.1$ (b1)–(b3), with $f_r = 0.1$ and $Re = 110$ (c1)–(c3), and with $f_r = 0.3$ (d1)–(d3).

$Nu_{mean} = 1.24$, 1.35, and 1.13 for $f_r = 0.1$, 0.18, and 0.3, respectively, when $Re = 110$ and $\theta = 1.5\pi$.

Given the minor differences in thermo-fluid dynamics between $Re = 100$ to 110 [see Figs. 14(b1)–14(b3) and Figs. 14(c1)–14(c3)], it is not surprising to see that the significant enhancement also occurs at $f_r = 0.1$ when $Re = 100$, rather than at other f_r considered in this study, as shown in Fig. 8(a). Under this condition, in the case with $f_r = 0.1$, large and strong vortices are exhibited, the velocity magnitude is enhanced, and a strong cold plume impinging on the hot wall at around $x = 6$, giving rise to a large local Nusselt number (Nu_{loc}), as shown in Figs. 13 and 14.

The enhancement of Nu_{mean} and Nu_{avg} when $f_r = 0.3$ is still remarkable, as shown in Fig. 13(a). This stems from the fact that the vortex shedding frequency f_v is equal to a quarter of f_r, i.e., $f_v = 0.075$, which is close to $f_v = 0.1$ when $f_r = 0.1$. As such, large and strong vortices and a cold plume are still also exhibited, enhancing the heat transfer performance, as shown in the last row of Fig. 14.

Generally for the same reason, when $\theta = \pi$, significant improvement can be attained at $f_r = 0.1$, compared to that in the corresponding stationary-plate case, as shown in Fig. 8(a).

4. Effects of θ

The above analysis shows that the major improvement is achieved usually when vortex synchronization or resonance occurs, for which the rotation frequency of the plate (f_r) should be sufficiently close or equal to the natural vortex shedding frequency (f_n) in the corresponding stationary-plate case. Since f_n varies with the orientation angle (θ), θ determines f_r at which vortex synchronization or resonance can occur, and thus the improvement. Specifically, when $Re \approx 100$, $f_n = 0.1$ for $\theta = 0$, $f_n = 0.25$ for $\theta = 0.5\pi$, and $f_n = 0.18$ for $\theta = \pi$ and 1.5π. Therefore, the enhancement can be attained roughly at around $f_r = 0.1$ to 0.25, as shown in Fig. 8(a).

Furthermore, θ influences the extent of the improvement in comparison to the corresponding stationary-plate cases. Particularly, for $\theta = 0$, π, and 1.5π, the flow, which nearly remains steady between the two steps in the stationary-plate cases, turns completely unsteady and induces strong vortex shedding when the plate rotates. Under this condition, significant improvement can be attained compared to the corresponding stationary-plate cases. The maximum enhancement of Nu_{mean} is around 95%, which is at $\theta = \pi$, as shown in Fig. 8(a). By contrast, much less improvement (around 8%) is attained for $\theta = 0.5\pi$, as strong vortex shedding occurs when the plate is stationary.

5. Effects of S

As revealed in Sec. III A, the heat transfer performance generally decreases with the horizontal distance of the plate from the BFS (S). This arises from the fact that the enhancement compared to the case without a plate is achieved mainly in the region from the plate to the FFS, which shrinks with S. This is also the case for the rotating-plate cases. Taking the cases with the orientation angle $\theta = 0$ and the rotation frequency $f_r = 0.1$ as an example, the improvement in the instantaneous spatial-averaged Nusselt number (Nu_{avg}) compared to the

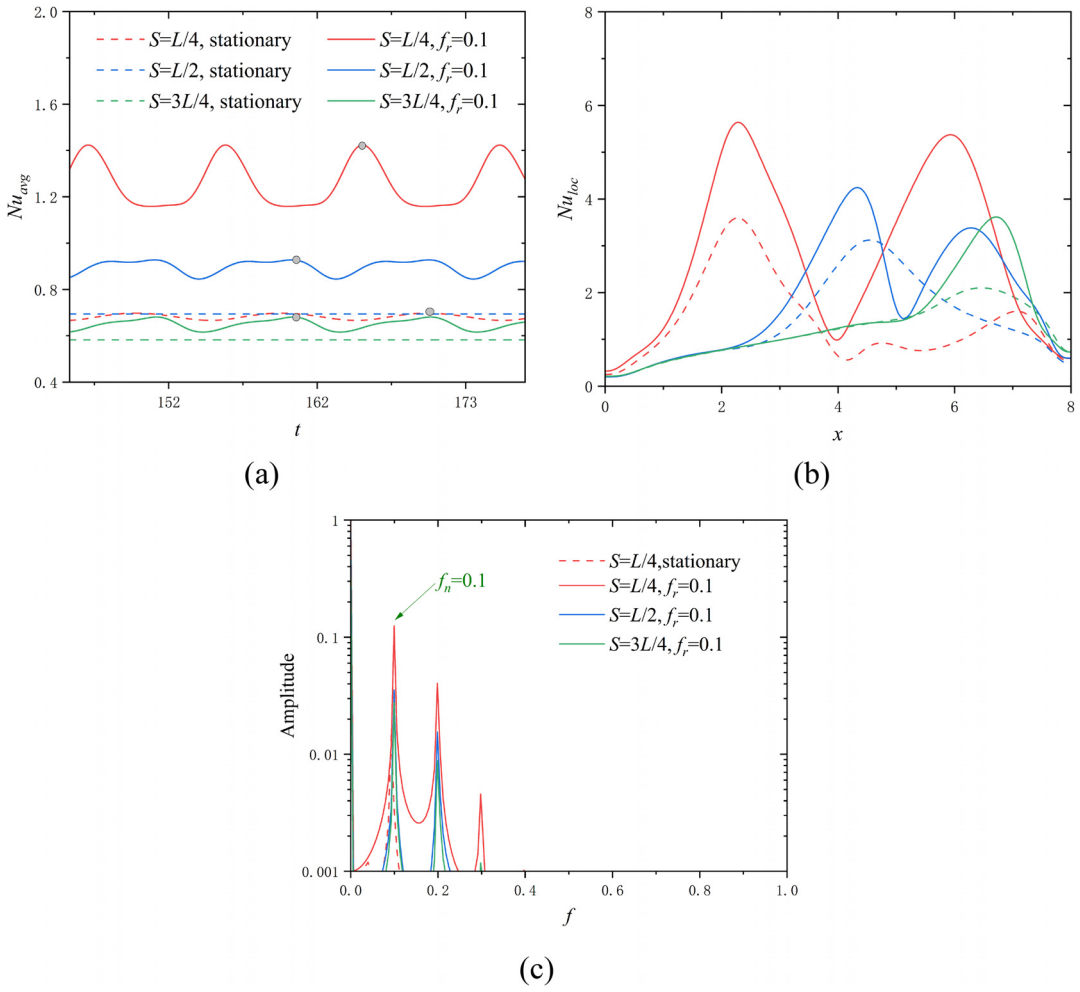

FIG. 15. Time history of the spatial-averaged Nusselt number (Nu_{avg}) (a) and the local Nusselt number (Nu_{loc}) along the bottom wall (b) in the case without a plate, with a stationary plate, and with a rotating plate for which $f_r = 0.1$ when $\theta = 0$ and $S = L/4$, $L/2$, and $3L/4$. Frequency spectra of Nu_{avg} in the stationary-plate case with $S = L/4$ and in the cases with $f_r = 0.1$ and $S = L/4$, $L/2$, and $3L/4$ (c). The solid symbols on the curves in panel (a) denote the instants selected for plotting the corresponding curves in panel (b).

corresponding stationary-plate cases decreases with S, as shown in Fig. 15(a). This is mainly attributed to the fact that the augmentation of the local Nusselt number (Nu_{loc}) is roughly attained in the region of $S < x < 8$, as shown in Fig. 15(b). Additionally, the enhancement of Nu_{loc} in this region also decreases with S, since the alternation of the flow by the rotating plate turns less obvious for a larger S, as shown in Fig. 16 and the first and second rows of Fig. 12. As such, the heat transfer performance also decreases with S in the rotating-plate cases, and so does the improvement.

IV. CONCLUSIONS

This study explores the influences of a rigid plate on the heat transfer performance of a channel with one BFS and one FFS in two scenarios. One is where a stationary plate is placed on the centerline of the channel with an orientation angle (θ) and a horizontal distance (S) from the BFS, while the other is where the plate with the same θ and S undergoes a sinusoidal rotation with the frequency (f_r). These two scenarios correspond to PFC and AFC, respectively. The main findings are summarized as follows:

- The heat transfer performance can be enhanced when the rigid plate is placed in the channel, no matter whether it is stationary or not. A better heat transfer performance can be achieved when the plate rotates rather than being stationary if θ and f_r are properly selected at all S.
- The enhancement can be achieved mainly when vortex synchronization or resonance occurs, i.e., when the natural vortex shedding frequency in the channel (f_n) in the stationary-plate case matches f_r in the corresponding rotating-plate case.
- The thermo-fluid dynamics is determined by θ, and so is f_n. Hence, θ affects f_r at which significant improvement can be achieved. For instance, when $S = L/4$, $f_r = 0.1$, and 0.25 can yield the greatest enhancement in the cases with $\theta = 0$ and 0.5π, as $f_n = 0.1$ and 0.25 in the corresponding stationary-plate cases, respectively.

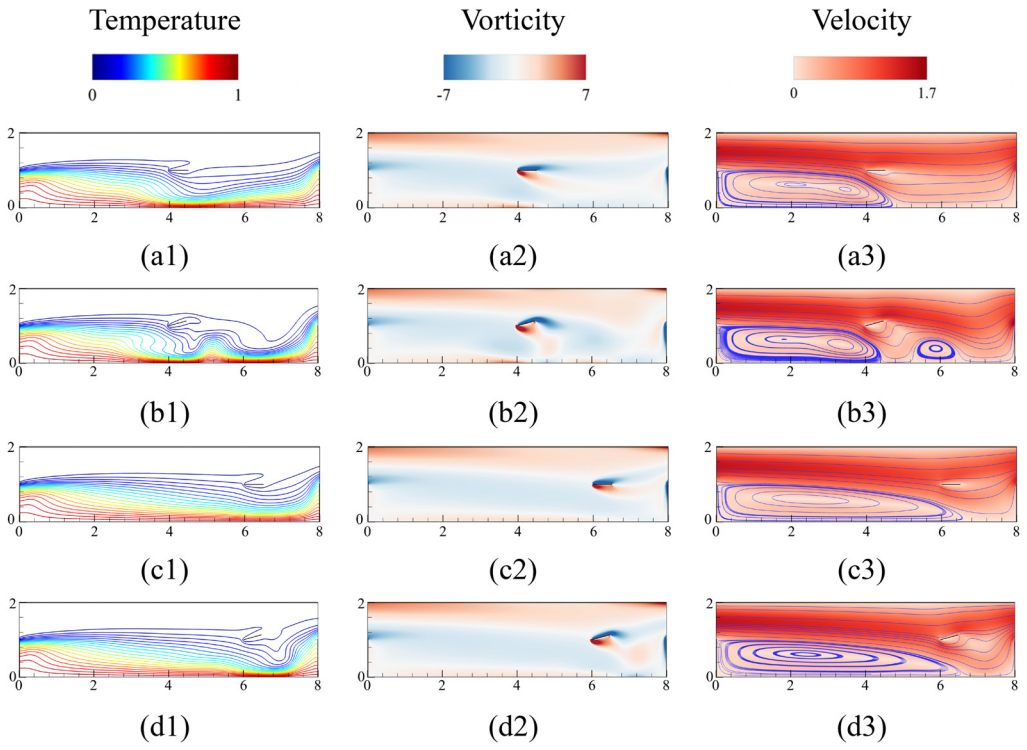

FIG. 16. Isothermal lines (the first column), vorticity contour (the second column), and streamlines and velocity contour (the third column) for the stationary-plate cases with $\theta = 0$ when $S = L/2$ (a1)–(a3) and $S = 3L/4$ (c1)–(c3), and for the rotating-plate cases with $f_r = 0.1$ when $S = L/2$ (b1)–(b3) and $S = 3L/4$ (d1)–(d3).

- No matter whether the plate is stationary or not, the heat transfer performance is primarily enhanced by the modification of thermo-fluid dynamics in the region between the plate and the FFS. Since the region shrinks with S, the enhancement reduces.

This study demonstrates that the heat transfer performance can be enhanced in the channel with the BFFS by a rigid plate when the PFC and AFC strategies are adopted. When θ and f_r are chosen properly, AFC outperforms PFC. Although promising, this study has some limitations since the effects of a few important factors are neglected. For instance, the Reynolds number and Richardson number, which could significantly affect the dynamics of the thermo-fluid system, are roughly fixed for simplicity. Additionally, the configuration of the channel also remains the same throughout this study. The influences of these factors would be considered in our near-future work.

ACKNOWLEDGMENTS

C.W. would like to acknowledge support from the Start-up and Postdoc Matching Funds of The Hong Kong Polytechnic University (Project Nos. P0035137 and P0036711), and from the Guangdong Basic and Applied Basic Research Foundation (Project No. 2021A1515110749).

AUTHOR DECLARATIONS

Conflict of Interest

The authors have no conflicts to disclose.

Author Contributions

Yuan Ma: Conceptualization (equal); Data curation (equal); Formal analysis (equal); Investigation (equal); Methodology (equal); Software (equal); Validation (equal); Visualization (equal); Writing – original draft (equal). **Feng Ren:** Formal analysis (equal); Investigation (equal); Writing – review & editing (equal). **Hui Tang:** Formal analysis (equal); Investigation (equal); Project administration (equal); Resources (equal); Supervision (equal); Writing – review & editing (equal). **Chenglei Wang:** Conceptualization (equal); Formal analysis (equal); Investigation (equal); Methodology (equal); Project administration (equal); Software (equal); Supervision (equal); Writing – review & editing (equal).

DATA AVAILABILITY

The data that support the findings of this study are available from the corresponding author upon reasonable request.

REFERENCES

[1]A. R. A. Talib and A. K. Hilo, "Fluid flow and heat transfer over corrugated backward facing step channel," Case Stud. Therm. Eng. **24**, 100862 (2021).
[2]S. Salman, A. A. Talib, S. Saadon, and M. H. Sultan, "Hybrid nanofluid flow and heat transfer over backward and forward steps: A review," Powder Technol. **363**, 448–472 (2020).
[3]C. Glaser, J. Hijlkema, J. Y. Lestrade, and J. Anthoine, "Influences of steps in hybrid rocket engines: Simulation and validation on simplified geometries," Acta Astronaut. **208**, 1–14 (2023).

[4]L. Gao and S. H. Bhavnani, "Experimental study of augmented flow boiling in a dielectric fluid due to backward and forward facing stepped microchannels," Int. J. Heat Mass Transfer **124**, 484–490 (2018).
[5]A. A. Memon, W. A. Khan, and T. Muhammad, "Numerical investigation of photovoltaic thermal energy efficiency improvement using the backward step containing Cu-Al_2O_3 hybrid nanofluid," Alexandria Eng. J. **75**, 391–406 (2023 Jul 15).
[6]P. Dehghan, F. Keramat, M. Mofarahi, and C. H. Lee, "Computational fluid dynamic analysis of graphene oxide/water nanofluid heat transfer over a double backward-facing microchannel," J. Taiwan Inst. Chem. Eng. **145**, 104821 (2023).
[7]S. Skullong, P. Promvonge, C. Thianpong, and M. Pimsarn, "Heat transfer and turbulent flow friction in a round tube with staggered-winglet perforated-tapes," Int. J. Heat Mass Transfer **95**, 230–242 (2016).
[8]M. Khoshvaght-Aliabadi, F. Hormozi, and A. J. Zamzamian, "Effects of geometrical parameters on performance of plate-fin heat exchanger: Vortex-generator as core surface and nanofluid as working media," Appl. Therm. Eng. **70**(1), 565–579 (2014).
[9]H. A. Mohammed, F. Fathinia, H. B. Vuthaluru, and S. Liu, "CFD based investigations on the effects of blockage shapes on transient mixed convective nanofluid flow over a backward facing step," Powder Technol. **346**, 441–451 (2019).
[10]C. Li, G. Cui, J. Zhai, S. Chen, and Z. Hu, "Enhanced heat transfer and flow analysis in a backward-facing step using a porous baffle," J. Therm. Anal. Calorim. **141**, 1919–1932 (2020).
[11]E. Jalil and G. R. Molaeimanesh, "Effects of turbulator shape, inclined magnetic field, and mixed convection nanofluid flow on thermal performance of micro-scale inclined forward-facing step," J. Cent. South Univ. **28**(11), 3310–3326 (2021).
[12]W. A. Xie and G. N. Xi, "Geometry effect on flow fluctuation and heat transfer in unsteady forced convection over backward and forward facing steps," Energy **132**, 49–56 (2017).
[13]A. Issakhov, Y. Zhandaulet, A. Abylkassyomova, M. Sakypbekova, and A. Issakhov, "Mixed convection in a channel with buoyancy force over backward and forward facing steps: The effects of inclination and geometry," Case Stud. Therm. Eng. **26**, 101152 (2021).
[14]M. Atashafrooz and S. A. Nassab, "Numerical analysis of laminar forced convection recess flow with two inclined steps considering gas radiation effect," Comput. Fluids **66**, 167–176 (2012).
[15]K. U. Rehman, W. Shatanawi, and A. B. Çolak, "Thermal analysis of flowing stream in partially heated double forward-facing step by using artificial neural network," Case Stud. Therm. Eng. **37**, 102221 (2022).
[16]A. K. Hilo, A. A. Iborra, M. T. Sultan, and M. F. Hamid, "Effect of corrugated wall combined with backward-facing step channel on fluid flow and heat transfer," Energy **190**, 116294 (2020).
[17]A. K. Hilo, A. A. Iborra, M. T. Sultan, and M. F. Hamid, "Experimental study of nanofluids flow and heat transfer over a backward-facing step channel," Powder Technol. **372**, 497–505 (2020).
[18]E. Abu-Nada, "Application of nanofluids for heat transfer enhancement of separated flows encountered in a backward facing step," Int. J. Heat Fluid Flow **29**(1), 242–249 (2008).
[19]Y. Ma, R. Mohebbi, M. M. Rashidi, Z. Yang, and Y. Fang, "Baffle and geometry effects on nanofluid forced convection over forward-and backward-facing steps channel by means of lattice Boltzmann method," Physica A **554**, 124696 (2020).
[20]S. Kumar and S. Vengadesan, "The effect of fin oscillation in heat transfer enhancement in separated flow over a backward facing step," Int. J. Heat Mass Transfer **128**, 954–963 (2019).
[21]H. Moayedi, "Numerical investigation of the effect of oscillating injection nanofluid flow on forced convection heat transfer enhancement over a backward-facing step," Eur. Phys. J. Plus **135**(11), 924 (2020).
[22]S. Kiwan, "Using localized wall discharge to control the fluid flow and heat transfer for the flow over a backward facing step," Int. J. Numer. Methods Heat Fluid Flow **18**(6), 745–765 (2008).
[23]F. Selimefendigil and H. F. Öztop, "Numerical investigation and reduced order model of mixed convection at a backward facing step with a rotating cylinder subjected to nanofluid," Comput. Fluids **109**, 27–37 (2015).
[24]F. Selimefendigil and H. F. Öztop, "Hydro-thermal performance of CNT nanofluid in double backward facing step with rotating tube bundle under magnetic field," Int. J. Mech. Sci. **185**, 105876 (2020).
[25]B. Calcagni, F. Marsili, and M. Paroncini, "Natural convective heat transfer in square enclosures heated from below," Appl. Therm. Eng. **25**(16), 2522–2531 (2005).
[26]S. Chen and G. D. Doolen, "Lattice Boltzmann method for fluid flows," Annu. Rev. Fluid Mech. **30**(1), 329–364 (1998).
[27]T. Krüger, H. Kusumaatmaja, A. Kuzmin, O. Shardt, G. Silva, and E. M. Viggen, *The Lattice Boltzmann Method* (Springer International Publishing, 2017).
[28]G. R. Kefayati and H. Tang, "Lattice Boltzmann simulation of viscoplastic fluids on natural convection in an inclined enclosure with inner cold circular/elliptical cylinders (Part I: One cylinder)," Int. J. Heat Mass Transfer **123**, 1138–1162 (2018).
[29]S. K. Kang, *Immersed Boundary Methods in the Lattice Boltzmann Equation for Flow Simulation* (Texas A&M University, 2010).
[30]C. Wang, H. Tang, S. Yu, and F. Duan, "Active control of vortex-induced vibrations of a circular cylinder using windward-suction-leeward-blowing actuation," Phys. Fluids **28**(5), 053601 (2016).
[31]C. Wang and H. Tang, "Influence of complex driving motion on propulsion performance of a heaving flexible foil," Bioinspiration Biomimetics **14**(1), 016011 (2018).
[32]Y. Ma, H. Tang, and C. Wang, "Enhancement of natural convection of a nanofluid by stress-free patches in an L-shaped enclosure," Int. J. Numer. Methods Heat Fluid Flow **33**(6), 2153–2180 (2023).
[33]J. Davalath and Y. Bayazitoglu, "Forced convection cooling across rectangular blocks," ASME. J. Heat Transfer **109**(2), 321–328 (1987).
[34]A. M. Aneesh, A. Sharma, A. Srivastava, and P. Chaudhury, "Effects of wavy channel configurations on thermal-hydraulic characteristics of printed circuit heat exchanger (PCHE)," Int. J. Heat Mass Transfer **118**, 304–315 (2018).
[35]F. Talebi, A. H. Mahmoudi, and M. Shahi, "Numerical study of mixed convection flows in a square lid-driven cavity utilizing nanofluid," Int. Commun. Heat Mass Transfer **37**(1), 79–90 (2010).
[36]A. Valencia and L. Hinojosa, "Numerical solutions of pulsating flow and heat transfer characteristics in a channel with a backward-facing step," Heat Mass Transfer **32**(3), 143–148 (1997).
[37]K. Khanafer, B. Al-Azmi, A. Al-Shammari, and I. Pop, "Mixed convection analysis of laminar pulsating flow and heat transfer over a backward-facing step," Int. J. Heat Mass Transfer **51**(25–26), 5785–5793 (2008).
[38]C. Wang, H. Tang, C. M. Simon, and F. Duan, "Lock-on of vortex shedding to a pair of synthetic jets with phase difference," Phys. Rev. Fluids **2**(10), 104701 (2017).
[39]C. H. Williamson and R. Govardhan, "Vortex-induced vibrations," Annu. Rev. Fluid Mech. **36**, 413–455 (2004).